VARIABLE TIMING CONTROL FOR ARCP VOLTAGE SOURCE INVERTERS OPERATING AT LOW DC VOLTAGE

Todd D. Batzel, Penn State Altoona; Kipp Adams, Penn State Altoona

Abstract

The Auxiliary Resonant Commutated Pole (ARCP) inverter has been of interest in motor drive applications that can benefit from any combination of increased conversion efficiency, reduced EMI radiation or higher PWM switching frequency. The ARCP inverter achieves high efficiency by turning the main switches on or off only under zero-voltage conditions. This reduces switching losses in the main circuit and potentially increases overall conversion efficiency. Furthermore, the reduced loss in the main switch allows for higher switching frequencies, which is of benefit for ironless low-inductance motors that are widely being used in small- to medium-power vehicle propulsion applications. The soft-switching ARCP generates an output with significantly reduced *dv/dt* and *di/dt* as compared to hard-switched inverters, which tends to reduce EMI emissions. All of these attributes of the soft-switching ARCP are beneficial in electric propulsion or electric vehicle auxiliary applications. In the ARCP inverter, the control signal timing for main and auxiliary switches is critical for maintaining the most favorable operating conditions. Many ARCP implementations utilize variable-timing control, where load current polarity and magnitude are used to determine the control signal timing–usually without additional sensors. In this study, the timing of main and auxiliary switching was examined for low dc bus voltage operation. A variable-timing methodology for ARCP switching was developed specifically in order to address issues associated with low-voltage ARCP operation. The operation principles are described here along with simulation and experimental results to demonstrate the approach.

Introduction

Auxiliary Resonant Commutated Pole (ARCP) technology was developed with the initial intent of reducing switching losses in the main switching devices of power conversion systems by switching them on or off only under zero-voltage conditions [1]. This soft-switching strategy also was intended to yield benefits such as reduced EMI emission [2-4] and permit operation of the switches at increased switching frequencies.

Although the adoption of the ARCP inverter tends to increase the overall cost and complexity of a drive system, its potential benefits make the ARCP of interest in a variety of electric vehicle (EV) applications. The ARCP inverter was proposed for electric vehicle propulsion by Dong et al. [5] and Morii et al. [6]. Dong et al. [5] demonstrated a significant efficiency benefit for an EV application with the use of an ARCP inverter operating with a DC bus voltage of 324 V. Similar results were obtained by Morii et al. [6] when they used an ARCP inverter suitable for high-power EVs.

There are two basic approaches used to generate the ARCP auxiliary and main switch control signals—fixed and variable timing. For the fixed-timing implementation, all switching times signals are generated using preset, constant values. Thus, fixed timing is easy to implement and has been shown to perform well over a limited range of load currents. However, fixed timing cannot produce zero-voltage switching (ZVS) for a wide load-current range. Variable-timing control was introduced by Chan et al. [7] to address this shortcoming of fixed timing, and uses the instantaneous load current to generate the switching signals that yield ZVS across the load-current range. Several studies have demonstrated improved ARCP efficiency for variable-timing control compared with the fixed-timing approach, with the increased performance coming at the expense of higher complexity [8-10]. Although voltage sensors placed across the switching devices are sometimes used to assist in ZVS implementation [11], their use significantly increases cost and complexity. Therefore, voltage sensors are generally avoided so that switching times must be determined in real-time using the circuit model and measured load current.

Although switching methodologies for ARCP inverters have been examined in the literature, published works in this area are aimed at high-voltage applications. In one such case, an ARCP inverter operating at 700 vdc showed improvement in efficiency when variable-timing control methods were employed [12]. In this current paper, the authors identify some of the issues that are specifically associated with low-voltage operation of the ARCP, and present a technique for implementation of variable-timing control under low-voltage conditions. In this study, simulations were performed and a prototype ARCP was operated at rela-

tively low voltages in order to demonstrate operation of the low-voltage system. The low-voltage range (24-42 V) is appropriate for small-vehicle propulsion applications and electric-vehicle auxiliaries such as power-steering assist.

ARCP Principle of Operation

The principle concept of the ARCP inverter is to force the voltage across main switches to be nearly zero volts before toggling their state. This has the effect of reducing the switching loss as compared to standard hard-switched configurations. An ARCP inverter configuration used to achieve this zero-voltage switching (ZVS) is shown in Figure 1 and it consists of two snubber capacitors (C_{r1} and C_{r2}) and a resonant branch added to a standard hard-switched pole. The resonant branch contains two auxiliary switches, *SP* and *SS*, for pumping current into or sinking current from the pole, respectively. Both the pump (*SP*) and sink (*SS*) auxiliary switches include anti-parallel diodes and a resonant inductor, L_r. The main pole was constructed with the main switches *S1* and *S2*, their associated flyback diodes and the aforementioned snubber capacitors.

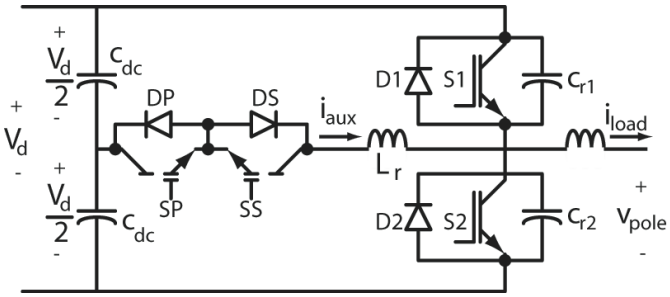

Figure 1. ARCP Pole Configuration

In order to operate the ARCP with the same conventional controllers as hard-switched inverters, the ARCP interface should be compatible with the standard PWM signals that are widely used in electric-machine control systems. The signals required to control the ARCP are shown in Figure 2, where the PWM input signal triggers the start of an ARCP state transition. Here, it is assumed that a logical 1 at the PWM input should deliver full DC bus voltage (V_d) to the pole output (V_{pole}), while a logical 0 should produce 0 V at the pole output.

In a hard-switched inverter, a rising PWM input signal turns off the lower switch (*S2*) and, following a short dead time, turns on the upper switch (*S1*). Similarly, a falling PWM input signal first turns off *S1*, then turns on *S2*. For ARCP soft-switching, where load current is to be commutated from a power switch to a diode (e.g., from *S1* to *D2* or *S2* to *D1*; see Figure 1), the hard-switched sequence can be used to obtain ZVS if the load-current magnitude is sufficient to charge or discharge the pole voltage from its current state to the opposite rail within switching time constraints. Otherwise, the auxiliary circuit must be used to introduce enough current to assist with the charge/discharge of the resonant capacitor. When switching load current from a diode to a switch or when load-current magnitude is small, the auxiliary circuit will always be used to assist the capacitor charge/discharge.

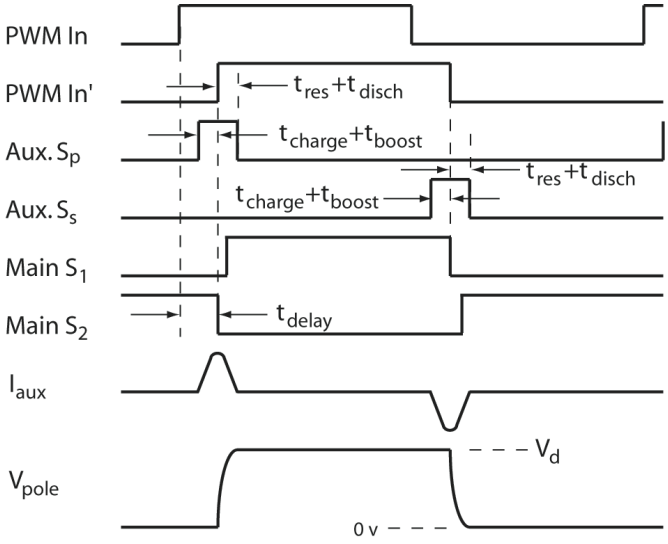

Figure 2. ARCP Signal Timing

Referring to Figure 2, ARCP operation when auxiliary current assist is necessary to commutate the load current from the lower diode (*D2*) to the upper switch (*S1*) is described as follows, where a positive load current i_{load} is assumed. A rising edge of the PWM input signal triggers the auxiliary pump switch (*SP*) so that the resonant inductor begins to charge. The time to charge the resonant inductor to the required current level (t_{charge} + t_{boost}) is variable and depends on the load-current level as well as the necessary boost current. When the auxiliary current (i_{aux}) magnitude exceeds the load current by a sufficient margin, called the boost current, i_{boost}, the bottom switch *S2* is turned off. With *S2* off, the boost current charges and discharges snubber capacitors C_{r2} and C_{r1}. In this case, the pole output voltage, v_{pole}, rises, while the slope of the auxiliary current decreases, eventually becoming negative. When C_{r1} is fully discharged, the upper switch, *S1*, is turned on at zero voltage. The resonant inductor continues to discharge toward zero current, at which point it will be turned off under zero-current conditions. The transitions for commutating load current from the upper switch (*S1*) back to the lower diode (*D2*) are similar.

Referring once again to Figure 2, it can be seen that for ARCP operation, the state change for the main switches occurs after some delay due to the resonant inductor charge time ($t_{charge} + t_{boost}$). To accommodate the maximum possible resonant inductor charge time delay, and to maintain compatibility with PWM controllers, a delayed PWM signal (PWM In') is generated. Therefore, the PWM input and delayed PWM input are offset by a delay (t_{delay}) corresponding to the maximum possible resonant inductor charge time, which has been expressed by Jiang [13] as:

In Equation (1), ${}^{'}I_{aux}$ is the maximum auxiliary current level required for the inverter operation, which is the rated load current plus the required boost current. Similarly, the required ramp time for charging the resonant inductor based on the variable load current is often determined using Equation (2):

$$t_{delay} = \frac{2{}^{'}I_{aux}L_r}{V_d} \tag{1}$$

$$t_{charge} + t_{boost} = \frac{2L_r}{V_d}\left(i_{load} + i_{boost}\right) \tag{2}$$

For variable-timing ARCP implementations, accurate prediction of the auxiliary current and pole output voltage state is essential for achieving zero-voltage (for main switches) or zero-current (for auxiliary devices) switching and, therefore, exploiting the ARCP benefits. For example, if the predicted auxiliary circuit charge time, ($t_{charge} + t_{boost}$), is longer than necessary, the resonant inductor will charge to an unnecessarily high current level resulting in increased auxiliary circuit conduction losses. Similarly, if the predicted auxiliary circuit charge time is shorter than necessary, the resonant inductor current may be insufficient to commutate the snubber capacitors to the opposite rail, and ZVS cannot be achieved.

The direct measurement of the auxiliary current is not easily or inexpensively incorporated into the ARCP controller. Therefore, for purposes of generating necessary timing signals, the auxiliary current dynamics are often computed [14] using Equation (3):

$$\frac{di_{aux}}{dt} = \frac{V_d - 2V_{pole}}{2L_r} \tag{3}$$

Likewise, in the absence of a voltage sensor, the voltage dynamics are characterized using the solution of Equation (3) along with the load-current measurement shown in Equation (4).

$$\frac{dv_{pole}}{dt} = \frac{1}{2c_r}\left(i_{aux} - i_{load}\right) \tag{4}$$

Low-Voltage ARCP Operation

In this section, the operation of the ARCP at low voltages is illustrated. Important aspects of operating the ARCP at low voltages are described along with the consequences of low-voltage operation relative to timing signal generation. Simulations are then used to substantiate the analysis.

Low-Voltage ARCP Operating States

For ARCP analysis and modeling, ideal-power switching device models have typically been used since, in high-voltage ARCP operation, those power device non-idealities are insignificant relative to the high operating DC bus voltage. For low-voltage operation, however, those power switch characteristics must be included in order to obtain ZVS through prediction of switching times. ARCP operation is now described using Figures 3 and 4, which show the ARCP signals and states, and the corresponding circuit for each state, respectively. In the interest of brevity, only a positive transition of the PWM input is considered. The load current is assumed to be positive so that the auxiliary circuit assist is necessary.

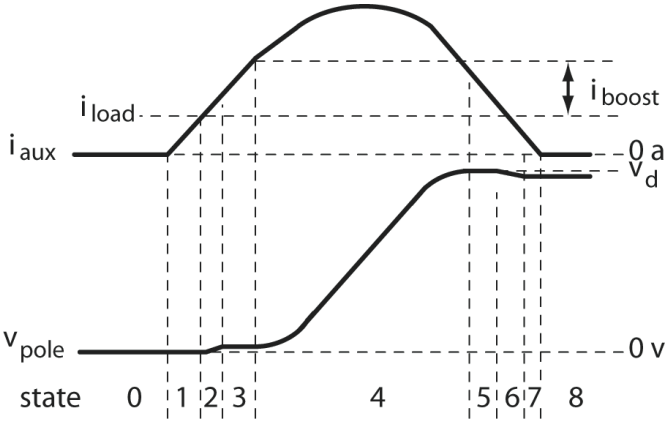

Figure 3. ARCP Signal Timing States, Including Switch Drops

The initial operating point in Figure 3 is state 0, which is a steady-state condition where *S2* is gated on, and *S1* off. Due to the load-current direction, diode *D2* is conducting the full load current, and the pole voltage output is the diode voltage drop, $-V_{d2}$. In this state, the auxiliary current is non-conducting and the resonant capacitors, C_{r1} and C_{r2}, are charged to V_d+V_{d2} and -V_{d2}, respectively.

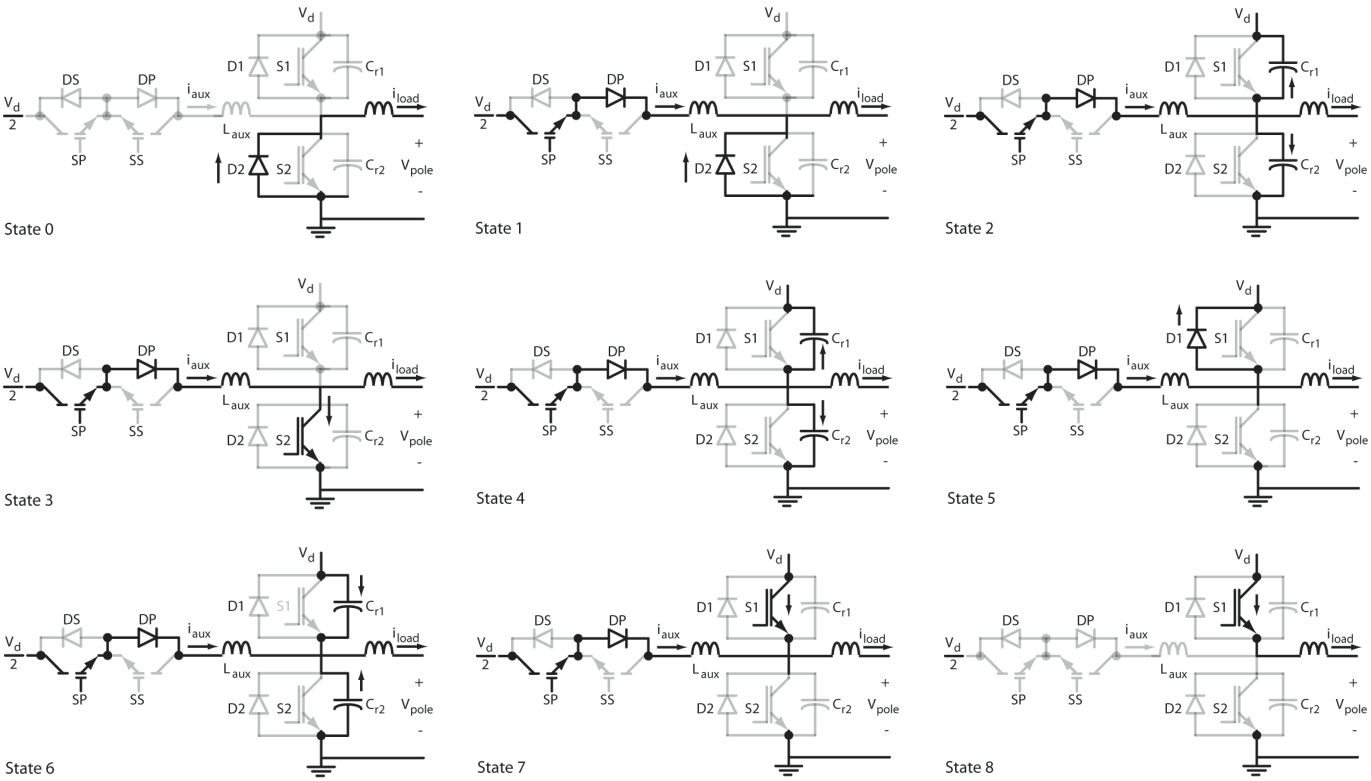

Figure 4. ARCP Turn-On States for Positive Load Current

The auxiliary pump switch (*SP*) turn-on marks the transition to state 1, as shown in Figure 3. Note in Figure 2 that there is an interval of between the PWM input edge and the auxiliary pump switch turn on. This interval depends on the amount of auxiliary current needed at the present operating point. In state 1, the resonant inductor will charge according to Equation (5), where v_{sa} and v_{da} represent the on-voltage drops of auxiliary circuit switches and diodes, respectively. As shown in Figure 4, the pole voltage in state 1 is clamped by load-current flow in *D2* to yield Equation 6.

$$\frac{di_{aux}}{dt} = \frac{1}{L_r}\left(\frac{v_d}{2} - \text{sgn}(i_{aux})(v_{sa} + v_{da}) - v_{pole}\right) \qquad (5)$$

$$\frac{dv_{c2}}{dt} = \frac{dv_{pole}}{dt} = 0 \qquad (6)$$

It is important to note the difference between Equation (5) and its approximation in Equation (3) that is often used for ARCP analysis. For high dc bus voltages, Equations (3) and (5) yield very similar results. However, for low dc bus voltages, their outcomes may differ significantly. State 1 persists until i_{aux} exceeds i_{load} and the ARCP transitions to state 2. At this point, diode *D2* turns off, and the difference between i_{aux} and i_{load} begins to charge c_{r2} until the capacitor voltage reaches the minimum turn-on voltage of the main switch, *S2*, which is $v_{ce,sat}$. In state 2, the auxiliary current is governed by Equation (5), while the pole voltage is described by Equation (4).

The changeover from state 2 to 3 occurs when c_{r2} is charged so that the main switch *S2* begins to conduct. In state 3, the main switch, *S2*, conducts the difference between the auxiliary and load current until this difference reaches a level (i_{boost}) sufficient to charge the resonant capacitor, c_{r2}, to the positive rail. In this state, the auxiliary current and pole-voltage equations obey Equations (5) and (6). When the resonant inductor is charged to the specified boost current level, *S2* is turned off and the ARCP transitions to state 4, as shown in Figures 3 and 4. With *S2* turned off, the boost current charges the resonant capacitors according to Equation (4), while the auxiliary current follows Equation (5). The timing for the turn-off of *S2* (or start of state 4) is of great importance: if it is turned off too late, unnecessary boost current and losses are introduced, while if it is turned off prematurely, it may not be possible for the resonant capacitor to be charged to the positive rail.

In state 4, as resonant capacitor c_{r2} charges, the auxiliary current will be reduced in slope according to Equation (5). It is also important to note that for auxiliary circuit pumping, the magnitude of di_{aux}/dt for rising versus falling auxiliary current will be different due to the voltage drops in the auxiliary and main switches. Thus, the auxiliary current charge and discharge will not be symmetric as originally predicted by Equation (3). The effect will be similar for auxiliary current sinking, during transitions from the upper diode (*D1*) to the lower switch (*S2*). For transitions from the upper switch (*S1*) to the lower diode (*D2*) at light positive load currents, or from the lower switch (*S2*) to the upper diode (*D1*) for light negative load currents, the asymmetry is even more pronounced. The asymmetry has implications in the calculation of optimum switching times for the auxiliary pump cycle that has not been addressed in previous works.

A transition to state 5 occurs when the pole voltage is fully charged and the boost current turns on *D1*. At (or near) this point, upper switch S1 can be turned on at zero voltage. Note, however, that *S1* will not conduct current until its turn -on voltage, $v_{ce,sat}$, is reached. In state 5, the auxiliary current continues to ramp toward zero according to Equation (5), and the pole voltage is determined from Equation (6). When i_{aux} falls below i_{load}, *D1* turns off and the difference in these currents will charge upper resonant capacitor c_{r1} until the turn-on voltage of *S1* is met. This corresponds to state 6 in Figures 3 and 4. In state 6, the pole voltage and auxiliary current are represented by Equations (4) and (5), respectively.

State 7 begins when c_{r1} is charged to a level sufficient to allow *S1* to begin conducting. In state 7, the load current is increasingly provided through *S1* as i_{aux} continues to decay toward zero. For this state, the pole voltage and auxiliary current are modeled by Equations (6) and (5), respectively. When i_{aux} fully discharges, marking the end of state 7, its control signal may be turned off at zero current. Since the auxiliary circuit will not conduct in the opposite direction (with *SS* off), this timing is not critical as long as the gate turn-off signal is applied *after* full discharge. When the resonant inductor is fully discharged, there is a transition to state 8, as shown in Figures 3 and 4. State 8 represents a steady state where switch *S*1 is on, *S*2 is off, the auxiliary current is again disabled and the output pole voltage is v_d-v_{s1} (for positive load current). The system will remain in state 8 until the input PWM signals the need to commutate the load current from the upper switch (*S1*) to the lower diode (*D2*).

A similar sequence was used to go from state 8 back to state 0 (upper switch to lower diode) for negative load current or small positive load current–the difference is that the auxiliary circuit branch sinks current in this case by turning on switch *SS*. However, similar procedures can be easily applied to identify state transitions for this case. In the interest of brevity, the details of these state transitions are not included in this discussion. For sufficiently negative load current, it is not necessary to use the auxiliary branch to commutate current from the lower diode to the upper switch since the load current itself can be used to charge the resonant capacitors to the opposite rail. Similarly, for sufficient positive load current, it is not necessary to use the auxiliary branch to sink current when transitioning from the upper switch to the lower diode.

Low-Voltage ARCP Experimental Results

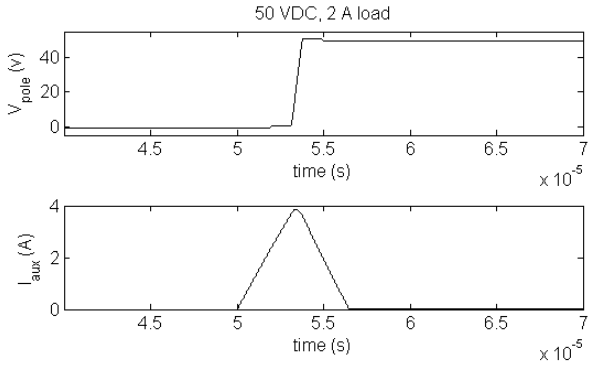

Figure 5. ARCP Simulation at 50 vdc and Pos. Load Current

In order to analyze low-voltage ARCP operation, a circuit simulation was performed. Example simulation results are shown in Figure 5, which shows operation at 50 vdc bus, and a positive load current of 1A. The simulation demonstrates some of the aspects of low-voltage ARCP operation as described previously. For example, the auxiliary current is asymmetric (auxiliary current rising slope is less than falling slope), as predicted by Equation (5).

Finally, to confirm simulations, an ARCP inverter pole pair (in H-bridge configuration) was constructed using IGBTs as the main switch and MCTs as the auxiliary switch. The system was programmed using variable-timing control. An example waveform showing auxiliary current and pole voltage from the experimental system is shown in Figure 6 for a positive load current of 1A and a dc bus voltage of 50 V. The experimental results show the same characteristics as the simulation.

Variable-Timing Control

In this section, the ARCP pole output voltage and auxiliary current signals are characterized for each ARCP state, and general solutions for the timing associated with each

state are developed. This analysis forms the basis for the variable-timing control of the ARCP.

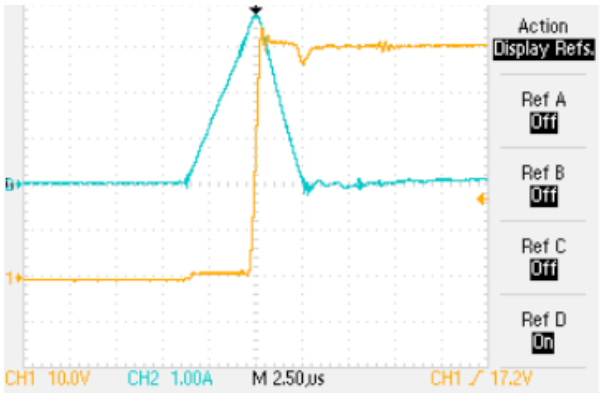

Figure 6. Experimental ARCP Aux. Current and Pole Voltage

ARCP Circuit Timing Analysis

The ARCP states shown in Figures 3 and 4 included two distinct operating modes. For states 2, 4 and 6, the circuit was in resonance mode. In states 1, 3, 5 and 7, the output voltage was clamped at some known value. Each of these operating modes of the ARCP was then analyzed to characterize the circuit timing.

1) *Resonant Circuit Timing Analysis*: The circuit was then analyzed for the resonant mode. The solution yielded timing characteristics for states 2, 4 and 6. Applying KCL to the circuit model for resonant mode shown in Figure 7 yielded Equations (7) and (8):

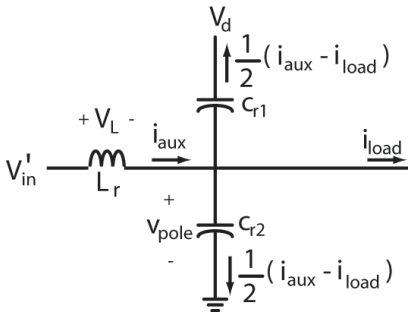

Figure 7. ARCP Equivalent Circuit for Resonance

$$V'_{in} - L_r \frac{di_{aux}(t)}{dt} - \frac{1}{2C_r}\int \left(i_{aux}(t) - i_{load}\right)dt = 0 \qquad (7)$$

$$V'_{in} = \frac{V_d}{2} - \text{sgn}\left(i_{aux}\right)\left(V_{da} + V_{sa}\right) - V_{pole,init} \qquad (8)$$

where $V_{pole,init}$ is the pole voltage at the start of each ARCP state, and V_{da} and V_{sa} represent the voltage drops across the auxiliary circuit diode and switch, respectively. The solution to Equation (7) is shown by Equation (9)

$$i_{aux}(t) = A\sin\left(\omega_0 t + \phi\right) + i_{load,init} \qquad (9)$$

where Equations (10) and (11) are

$$\omega_0 = \sqrt{\frac{1}{2L_rC_r}} \qquad (10)$$

$$A = \sqrt{\frac{2C_r}{L_r}V'^2_{in} + \left(i_{aux,init} - i_{load}\right)^2} \qquad (11)$$

and $i_{aux,init}$ represents the auxiliary current at the start of the ARCP state of interest. Also,

$$\phi = \sin^{-1}\left(\frac{i_{aux,init} - i_{load}}{A}\right) \quad \text{for } V'_{in} \geq 0 \qquad (12)$$

or

$$\phi = \pi - \sin^{-1}\left(\frac{i_{aux,init} - i_{load}}{A}\right) \quad \text{for } V'_{in} < 0 \qquad (13)$$

With the auxiliary current known from Equation (9), the pole voltage output can be determined from Equation (14):

$$V_{pole}(t) = V'_{in} - L_r\frac{di_{aux}}{dt} \qquad (14)$$

Differentiating Equation (9) and plugging it into Equation (14) gives us

$$V_{pole}(t) = V'_{in} - B\cos\left(\omega_0 t + \phi\right) + v_{pole,init} \qquad (15)$$

where

$$B = \sqrt{V'^2_{in} + \frac{L_r}{2C_r}\left(i_{aux,init} - i_{load}\right)^2} \qquad (16)$$

Finally, Equation (15) was solved for each possible time for which the pole voltage, $V_{pole}(t)$ would take on the value $\overline{V}_{pole}$, given the initial conditions; see Equation (17):

$$t_{rv} = \frac{1}{\omega_0}\left[\pm\cos^{-1}\left(\frac{V'_{in} + v_{pole,init} - \overline{V}_{pole}}{B}\right) - \phi + 2\pi n\right] \qquad (17)$$

This yielded (for n=0, 1, 2, …) all possible times for which the pole voltage would have the specified magnitude. For

the ARCP application where resonance is not sustained, the authors were interested in the solution with the smallest positive time from Equation (17).

2) *Clamped Circuit Timing Analysis*: For ARCP states 1, 3, 5 and 7, the output voltage of the ARCP was clamped so that the circuit was not in resonance. With the voltage clamped, one can easily solve for the time required for the auxiliary current to reach a target value, $\bar{I}_{aux}$, given the initial condition of Equation (18):

$$t_{ci} = \frac{L_r\left(\bar{I}_{aux} - i_{aux,init}\right)}{V'_{in}} \tag{18}$$

Variable Timing

Using the solutions from the previous section, each of the ARCP states described in Figures 3 and 4 were then analyzed to quantify their respective state times. By knowing the timing characteristics of each state, the required switching times for the main and auxiliary switches can be predicted and applied to variable-timing control. It should be noted, once again, that the following analysis was performed for a positive load current and for the commutation of current from the lower diode (*D2*) to the upper switch (*S1*). Other transitions can be analyzed using the same procedure.

ARCP state 1 has the output voltage clamped to $-v_{d2}$, an initial auxiliary current of zero, and a target auxiliary current equal to the load current. Therefore, Equation (18) was used to find the total time required for ARCP state 1:

$$t_1 = \frac{L_r i_{load}}{v'_{in}} \tag{19}$$

ARCP state 2 was a resonant state where the initial pole voltage was $-v_{d2}$, and the pole voltage at the end of this state would be v_{s2}. Therefore, Equation (17) was used to determine the total time required for ARCP state 2:

$$t_2 = \frac{1}{\omega_0}\left[\pm\cos^{-1}\left(\frac{V'_{in} - v_{D2} - v_{ce,sat}}{B}\right) - \phi + 2\pi n\right] \tag{20}$$

Once the total time for state 2 was determined, it could be used with Equation (9) to find the auxiliary current at the end of state 2:

$$i_{aux}(t'_2) = \sqrt{\frac{2C_r}{L_r}V'^2_{in}}\,\sin\left(\omega_0 t_2\right) + i_{load} \tag{21}$$

For ARCP state 3, the resonant capacitor was clamped by a conducting *S2*. The initial auxiliary current was given by Equation (21), and the final auxiliary current was the load current plus the required boost current. Thus, using Equation (19) gives:

$$t_3 = \frac{L_r\left(i_{load} + i_{boost} - i_{aux}(t'_2)\right)}{V'_{in}} \tag{22}$$

Next, ARCP state 4 was examined, for which the pole voltage resonates from an initial value of v_{s2} to a final value of $v_d + v_{d1}$. From Equation (17), it was found that

$$t_4 = \frac{1}{\omega_0}\left[\pm\cos^{-1}\left(\frac{V'_{in} + v_{s2} - (v_d + v_{d1})}{B}\right) - \phi + 2\pi n\right] \tag{23}$$

The corresponding auxiliary current at the end of t_4 was

$$i_{aux}(t'_4) = \sqrt{\frac{2C}{L_r}V'^2_{in} + i^2_{boost}}\,\sin\left(\omega_0 t_4 + \phi\right) + i_{load} \tag{24}$$

For ARCP state 5, the auxiliary current decayed from its initial value given by Equation (24) to a final value that was equal to the load current. During this time, the pole voltage was clamped to the DC bus voltage plus the diode voltage drop. The time for auxiliary current to decay is

$$t_5 = \frac{L_r\left(i_{load} - i_{aux}(t'_4)\right)}{V'_{in}} \tag{25}$$

The total time for ARCP state 6 was computed using Equation (17) from the initial pole voltage of $v_d + v_{d1}$ to its value when upper switch *S1* begins to conduct, which was $v_d - v_{ce,sat}$.

$$t_6 = \frac{1}{\omega_0}\left[\pm\cos^{-1}\left(\frac{V'_{in} + v_{D1} + v_{ce,sat}}{B}\right) - \phi + 2\pi n\right] \tag{26}$$

The auxiliary current at the end of t_6 was obtained from the auxiliary current at the start of the state, which was i_{load}:

$$i_{aux}(t'_6) = \sqrt{\frac{2C_r}{L_r}V'^2_{in}}\,\sin\left(\omega_0 t_6 + \phi\right) + i_{load} \tag{27}$$

Finally, ARCP state 7 time, where the auxiliary current ramps to zero with the pole voltage clamped at $v_d - v_{ce,sat}$ was computed using Equation (18):

$$t_7 = \frac{L_r\left(-i_{aux}(t'_6)\right)}{v'_{in}} \tag{28}$$

At the end of state 7, the auxiliary switch was turned off at zero current and the ARCP was in a steady state with the upper switch (*S1*) conducting the full load current.

Variable-Timing Control for Low-Voltage ARCP

Lai et al. [11] showed that variable-timing control of the ARCP was critical for optimizing the inverter performance–specifically in minimizing losses in the power switching components and avoiding damaging transient currents. The ARCP timing results from the previous section were then used to determine optimum switching times for auxiliary and main switches.

Referring to Figure 2, the fixed delay time, t_{delay}, between the input PWM signal transition and the turn off of main switch *S2* first had to be computed. This delay is necessary to allow sufficient time for the auxiliary current to reach its required level before switching the state of any main switches. Although Equation (1) has been used in the literature, it may not allow sufficient time when considering voltage drops in the auxiliary circuit. Therefore, a more accurate computation applicable to low-voltage ARCP operation would be given as Equation (29):

$$t_{delay} = \frac{L_r \hat{I}_{aux}}{0.5v_d - v_{sa} - v_{da}} \tag{29}$$

Next, referring to Figure 2, auxiliary switch *SP* is turned on, $t_{charge} + t_{boost}$, before main switch *S2* is turned off. Noting that t_{charge} and t_{boost} correspond to ARCP states 1-3, the time from the PWM-In signal until the auxiliary switch *SP* is turned on was determined by Equation (30):

$$t_{SP,ON} = t_{delay} - \sum_{n=1}^{3} t_n \tag{30}$$

From Figure 2, it can be seen that the lower switch (*S2*) is turned off exactly t_{delay} after the PWM In signal:

$$t_{S2,OFF} = t_{delay} \tag{31}$$

The upper switch (*S1*) can be turned on at zero voltage at

$$t_{S1,ON} = t_{delay} + t_4 \tag{32}$$

Finally, the auxiliary pump switch, *SP*, can be turned off at zero current no sooner than

$$t_{SP,OFF} = t_{delay} + \sum_{n=4}^{7} t_{state\ n} \tag{33}$$

ARCP Simulation Results

In this section, the ARCP timing analysis presented previously is compared with more traditional variable-timing approaches. In addition, simulations of a low-voltage variable-timing ARCP inverter using these results are performed.

Variable-Timing Comparison

The ARCP variable-time computation methodology presented in the previous section was then compared to other techniques that have been reported in the literature. The results are summarized in Figure 8. For purposes of comparison, the resonant inductor and capacitor values were adjusted in proportion, and in inverse proportion to the dc voltage, respectively, so that the calculated times would be constant using the conventional calculation method.

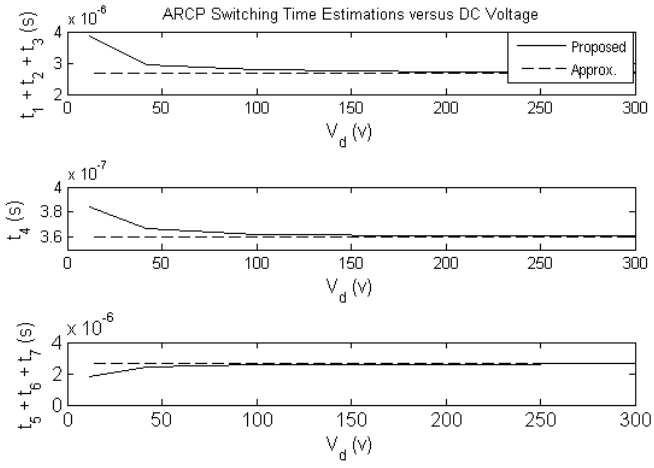

Figure 8. Switching Time Calculations for 1A Load

The first variable-timing parameter to be compared was the time required for the auxiliary current to be charged to the load current plus the required boost current level. In this study, that time corresponded to $t_1 + t_2 + t_3$, from Equations (19), (20) and (22), whereas other published works [15], [16] used Equation (2). Figure 8 shows that these two computations produce results that correspond closely at high dc bus voltages, yet diverge significantly at low voltages due to the significance of device non-idealities that are not considered in Equation (2). The significance of this computation is that it is used to determine the time at which the lower switch is to be turned off in order to end the charging of the auxiliary inductor. Too short a charge time could result in insufficient boost current to resonate the pole output voltage to the opposite rail, whereas too long a charging time would yield excessive boost current that could unnecessarily in-

crease the total ARCP commutation time and increase the conduction losses.

Next, the resonant time (t_4), as described in Equation (23), was compared with the computation suggested by Kuhn and Sudhoff [15]:

$$t_{res} = \frac{2}{\omega_0} \tan^{-1}\left(\frac{C_r \omega_0 V_d}{i_{boost}}\right) \tag{34}$$

Once again, Figure 8 shows that the results were similar only at high dc voltages. The time required for the auxiliary current to decay to zero after the completion of the resonant phase ($t_5 + t_6 + t_7$) as specified in Equations (25), (26) and (28) was compared to the method used by Kuhn and Sudhoff [15]. Figure 8 also shows good agreement except at low dc voltages, as expected. The comparison shown in Figure 8 corresponds to ARCP transitions from the lower diode to the upper switch with positive load current. However, examination of other ARCP transitions yielded similar results to those of Figure 8.

ARCP Simulation

An ARCP circuit simulation was then used to compare computed timing characteristics to those obtained from the simulation. The simulation utilized a low bus voltage of 28V dc, C_r = 10,000 pf, L_r = 18 μH and a positive load current of 1A. The boost current was set to 1.5A. The result of a transition from the lower diode to the upper switch is shown in Figure 9.

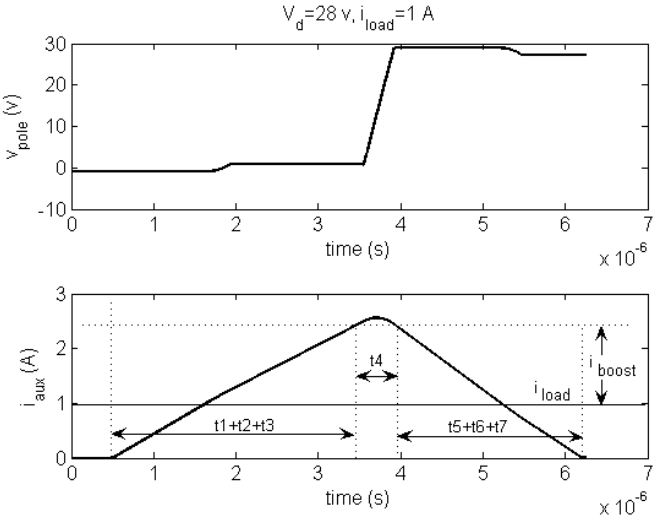

Figure 9. ARCP Simulation for Low DC Bus Voltage, 1A Load

A close examination of the circuit simulation shows that the time for the auxiliary current to reach the load-current level plus the boost current (as measured from the auxiliary pump switch turn-on) was 3.053 μsec. This compares quite favorably with the computed value from Equations (19), (20) and (22) of 3.076 μsec. However, the traditional calculation methodology yielded 2.678 μsec. Thus, if the traditional methodology were to be applied to this low-voltage ARCP with variable-timing control, the lower switch would be turned off before the required boost current is reached. This could result in loss of zero-voltage switching.

The circuit simulation showed a resonant time (t_4) of 0.379 μsec, compared to the computed time from Equation (23) of 0.3698 μsec. The traditional calculation method yielded a resonant time of 3.598 μsec. Finally, the total time for the ARCP commutation as measured from the turn-on of the auxiliary pump switch to the instant the auxiliary current decayed to zero was observed to be 5.699 μsec in the simulation. The computed value using Equations (19), (20), (22), (23), (25), (26) and (28) was 5.71 μsec, while the traditional computation yielded 5.64 μsec.

Conclusion

In this paper, the authors presented a variable-timing method for accurate soft-switching in an ARCP converter over a wide dc bus voltage range. It was shown through simulation that special attention is needed for accurate timing control of the ARCP when the dc bus voltage is low (where low is defined generally as the voltage level at which the switching device voltage drops play a significant role in the circuit). This proposed approach was verified through simulation to be accurate in determining appropriate gate switching times required to optimize performance of the ARCP. The switching times determined using the proposed approach were also compared to approaches where the device voltage drops were not considered to demonstrate the potential implications of low-voltage ARCP operations on variable timing.

References

[1] De Doncker, R. W., & Lyons, J.P. (1990). The Auxiliary Resonant Commutated Pole Converter. *IEEE Industry Applications Society Annual Meeting*, *2*, 1228-1235.

[2] Zhu, H., Lai, J., Hefner, A.R., Tang, Y., & Chen, C. (2001). Modeling-Based Examination of Conducted EMI Emissions from Hard and Soft-Switching PWM Inverters. *IEEE Transactions on Industry Applications, 37*(5), 1383-1393.

[3] Emami, Z., Farzanefard, H., & Motahari, S. R. (2010). EMI Evaluation in Hard Switching and Soft Switching PWM Flyback Converters. *Power Electronic & Drive Systems & Technologies Conference (PEDSTC)*, (pp. 46-51).

[4] Kim, H. J., Chung, Y. H., Lee, K. S., Jon, Y. S., & Kim, K. S. (2007). Performance Analysis of Soft-Switching Inverter for the Photovoltaic Power System. *7th International Conference on Power Electronics*. (pp. 436-439).

[5] Dong, W., Choi, J., Li, Y., Yu, H., Lai, J., Boroyevich, D. et al. (2000). Efficiency Considerations of Load Side Soft-Switching Inverters for Electric Vehicle Applications. *Applied Power Electronics Conference and Exposition, 2*, 1049-1055.

[6] Morii, H., Yamamoto, M., & Funabiki, S. (2009). Capacitor-Less Auxiliary Resonant Commutated Pole (ARCP) Voltage Source Soft Switching Inverter Suitable for EV. 13th *European Conference on Power Electronics and Applications,* (pp. 1-8).

[7] Chan, C. C., Chau, K. T., Chan, D. T. W., Yao, J., Lai, J., & Li, Y. (1998). Switching Characteristics and Efficiency Improvement with Auxiliary Resonant Snubber Based Soft-Switching Inverters. *Power Electronics Specialists Conference* '98, *1*, 429-435.

[8] Yu, Q., & Nelms, R. M. (2002). State Plane Analysis of an Auxiliary Resonant Commutated Pole Inverter and Implementation with Load Current Adaptive Fixed Timing Control. *IECON*, *1*, 437-443.

[10] Lai, J., Zhang, J., Yu, H., & Kouns, H. (2006). Source and Load Adaptive Design for a High-Power Soft-Switching Inverter. *IEEE Transactions on Power Electronics*, *21*(6), 1667-1675.

[11] Lai, J., Yu, W., & Park, S. (2009). Variable Timing Control for Wide Current Range Zero-Voltage Soft-Switching Inverters. *24th Annual IEEE Applied Power Electronics Conference and Expo*, (pp. 407-412).

[12] Ma, K., Xu, D., Zhang, T., & Igarashi, L. (2009). The Evaluation of Control Strategies for Auxiliary Resonant Commutated Pole Inverter. *IEEE Energy Conversion Congress and Exposition*, (pp. 810-816).

[13] Jiang, J., Zhou, X., & Zhang, W. (2000). An Improved Auxiliary Resonant Commutated Pole Inverter Using Assistant Power Source. *3rd International Power Electronics and Motion Control Conference*, *1*, 158-162.

[14] Walters, E. A., Pekarek, S. D., & Wasynczuk, O. (1997). Simulation of an ARCP-Based Field Oriented Induction Motor System. *Proceedings of the Naval Symposium on Electric Machines*, (pp. 85-90).

[15] Kuhn, B. T., & Sudhoff, S. D. (1997) Modeling Considerations in ARCP Versus Hard Switched Drives. *Proceedings of the 1997 Naval Symposium on Electric Machines*, (pp. 161-168).

[16] Teichmann, R., & Bernet, S., (1998). Investigation and Comparison of Auxiliary Resonant Commutated Pole Converter Topologies. *29th Annual IEEE Power Electronics Specialists Conference Record*, *1*, 15-23.

Biographies

TODD D. BATZEL received a BS in electrical engineering from Pennsylvania State University in 1984, an MS in electrical engineering from the University of Pittsburgh in 1989, and a PhD in electrical engineering in 2000 from Pennsylvania State University. He is currently an associate professor of electrical engineering at Penn State Altoona. His research interests include machine controls, electric drives, and artificial intelligence. Dr. Batzel may be reached at tdb120@psu.edu

KIPP ADAMS is currently a fourth-year student in the electro-mechanical engineering technology program at Penn State Altoona.